mater.scichina.com link.springer.com

Published online 11 December 2023 | https://doi.org/10.1007/s40843-023-2673-6
Sci China Mater 2024, 67(1): 76–84

Improving the cycling stability of lithium-ion batteries with a dry-processed cathode *via* the synergistic effect of carboxymethyl cellulose and siloxane

Minghan Ni[1,3], Yang Zhao[1,3], Nuo Xu[1,3], Mengxin Kong[4], Yanfeng Ma[1,3], Chenxi Li[1,3], Hongtao Zhang[1,3*] and Yongsheng Chen[1,2,3]

ABSTRACT **The solvent-free dry process for fabricating battery electrodes has received widespread attention owing to its low cost and environmental friendliness. However, the conventional polytetrafluoroethylene (PTFE) used as a binder in the preparation of dry-processed electrodes results in insufficient adhesion, limiting their practical industrial applications. Herein, we reported an industrially viable dry process for producing lithium-ion batteries using the combination of carboxymethyl cellulose (CMC) and siloxane as the binder composite. The synergistic effect of CMC and siloxane enhanced the adhesive performance of the electrode, thereby improving the mechanical strength and electrochemical performance of the developed dry-processed electrode. Half cells based on aluminum-doped lithium manganese oxide (LMA) dry-processed electrodes with CMC and siloxane (LMA/CS) exhibited a capacity retention of 79.8% after 200 cycles at 1 C. Furthermore, LMA/CS||lithium titanate oxide full cells with a high mass loading of 20.6 mg cm^{-2} demonstrated an excellent capacity retention of 89.2% after 1000 cycles, which is considerably higher than that of cells based on slurry-processed electrodes prepared with a polyvinylidene fluoride binder and conventional dry-processed electrodes prepared using a PTFE binder.**

Keywords: lithium-ion batteries, dry process, binder, high performance, siloxane

INTRODUCTION

Lithium-ion batteries (LIBs) have emerged as the next generation of energy-storage devices owing to their high energy density and excellent cycling stability [1–4]. Currently, the predominant method for the mass production of LIBs includes the conventional slurry-based approach [5]. This method involves coating metallic current collectors with a well-dispersed slurry consisting of a mixture of active material particles, conductive additives, and polyvinylidene fluoride (PVDF) binder dissolved in *N*-methyl-2-pyrrolidone (NMP) [6,7]. However, slurry processes feature increased costs and energy consumption. The wet coating and subsequent drying/solvent recovery processes account for ~48.2% of the total energy expenditure and up to ~27.5% of the total manufacturing cost, respectively [8–11]. There are concerns about the toxicity of NMP [12] and the need for strict humidity control due to the reactivity of PVDF/NMP with water [13]. In addition, PVDF exhibits limited flexibility and a low elongation rate (only 5%) [14]. Moreover, during the drying process, capillary action and diffusion effects would result in crack formation, particularly in thicker electrodes [15]. These limitations restrict the electrode thickness and fail to meet the requirements for realizing batteries with extended cycle life. Therefore, various strategies have been developed to explore alternative approaches for manufacturing LIB electrodes that circumvent the issues associated with slurry processes.

The solvent-free dry process is considered a promising alternative to the conventional slurry-processed electrode fabrication method, primarily owing to its excellent cost effectiveness and energy efficiency [6,16]. Moreover, the dry process enables precise control over electrode thickness and uniformity for thick electrodes, resulting in reduced crack formation and a smoother surface [17,18]. Consequently, this approach enables the fabrication of higher mass-loading electrodes suitable for practical applications and improves the energy density of LIBs. To date, dry-processed electrodes have mainly used polytetrafluoroethylene (PTFE) as the representative polymer binder [19,20]. PTFE is characterized by high chemical and thermal resistance and excellent mechanical properties [13]. It forms a fibrous linear binding structure with active materials and conductive additives [21]. However, the weak van der Waals forces among the molecular chains of PTFE make it unsuitable for accommodating the volume fluctuations of active materials during cyclic processes [15]. Moreover, undesired potential side reactions would occur between PTFE and the electrolyte. In particular, the decomposition of lithium salt and PTFE contributes to the formation of cathode electrolyte interphase (CEI) and can affect the binding performance within the electrode [22]. Therefore, exploring more effective binders or crosslinking agents to improve the bonding performance of PTFE in dry-processed electrodes is vital.

[1] The Centre of Nanoscale Science and Technology and Key Laboratory of Functional Polymer Materials, Institute of Polymer Chemistry, College of Chemistry, Nankai University, Tianjin 300071, China
[2] State Key Laboratory of Elemento-Organic Chemistry, Nankai University, Tianjin 300071, China
[3] Renewable Energy Conversion and Storage Center (RECAST), Nankai University, Tianjin 300071, China
[4] Tianjin Plan Nano Co., Ltd, Tianjin 300071, China
* Corresponding author (email: htzhang@nankai.edu.cn)

Carboxymethyl cellulose (CMC), a widely used and efficient aqueous binder, exhibits sufficient hydroxyl groups that allow it to bond with other electrode components through noncovalent interactions and preserve the integrity of the whole electrodes [23–25]. Numerous studies have confirmed the significant potential of CMC to replace traditional PVDF or PTFE binders. Lux *et al.* [26] reported that the homogenous distribution of CMC can improve the long-term cycling stability of $LiFePO_4$/CMC electrodes. Additionally, the carboxyl acid groups on Na-CMC can participate in the formation of the solid electrolyte interface on graphite anodes, thereby improving the long-term cycling performance of graphite/Na-CMC anodes [27]. Furthermore, siloxane crosslinkers, such as bis[(3-methyldimethoxysilyl) propyl] epoxy propane, contain hydrolyzable groups on their silicon atoms, which can undergo hydrolysis to form hydroxyl groups, thereby enabling the formation of a Si–O–Si crosslinked network [28]. Previous studies have investigated the use of polydimethylsiloxane terminated with $-OCH_3$ groups and poly(imide-*co*-siloxane) as adhesion additives to enhance the mechanical properties, electrical/thermal stability, and cycling performance of electrodes [29–31]. The interactions between siloxane crosslinkers and metal oxides facilitate the uniform distribution of active materials within the electrodes, along with the formation of a three-dimensional (3D) flexible network [32,33]. Therefore, CMC and siloxane can enhance the performance of the PTFE binder in dry-processed electrodes.

Herein, we proposed a simple and scalable approach for preparing dry-processed electrodes with high mass loadings. This method involved a two-step rolling technique using a siloxane–CMC–PTFE binder composite (Fig. 1a), which is suitable for industrial production [34]. The presence of abundant functional groups, such as –OH and –COOH, in CMC promoted the formation of hydrogen bonds with the surface of the active materials. In addition, the hydrophobic segments of CMC can interact with the hydrophobic PTFE chain to enhance the dispersion of components and reduce electrical contact losses [35]. Furthermore, the siloxane crosslinker formed a flexible Si–O–Si 3D network capable of accommodating volume changes during cycling and mitigating the pulverization of cathode materials and capacity degradation. Consequently, half cells constructed using dry-processed lithium manganese oxide cathodes incorporating the CMC–siloxane binder composite (LMA/CS) exhibited an excellent capacity retention of 79.8% after 200 cycles at a rate of 1 C. Moreover, full cells (LMA/CS|| lithium titanate oxide) with a high mass loading of 20.6 mg cm^{-2} demonstrated excellent long-cycling performance, retaining 89.2% of their capacity after 1000 cycles at 1 C. This performance considerably surpasses that of traditional slurry-processed electrodes.

EXPERIMENTAL SECTION

In a typical process, we prepared an agglomerate by blending LMA, Ketjen Black (KB), CMC, bis[(3-methyldimethoxysilyl)-propyl] epoxy propane (siloxane) (the chemical structure in Fig. S1), and PTFE in a mortar. Subsequently, the agglomerate was rolled to create a self-supporting film. Finally, the self-supporting film was loaded onto carbon-coated aluminum foil between two rollers to form an electrode sheet under heating conditions (Fig. 1a). The preparation process of the LMA/PTFE electrode was similar to that of the LMA/CS electrode without the addition of CMC and siloxane. Further experimental details of the preparation process are provided in the Supplementary information.

RESULTS AND DISCUSSION

Characterization of the LMA/CS and LMA/PTFE electrodes

During the preparation process, the LMA/CS electrode films exhibit visually smooth and crack-free surfaces, as confirmed by optical photographs (Fig. 1b). The structural composition of the LMA/CS electrode is shown in Fig. 1c. CMC, a conventional linear binder, exhibits a strong capacity for forming hydrogen bonds and establishes a strong connection with active materials, conductive additives, and binders through noncovalent interactions. These interactions considerably enhance the dispersibility of these components. Under elevated temperature conditions, siloxane readily forms a Si–O–Si network. This network effectively constrains the volumetric variation and

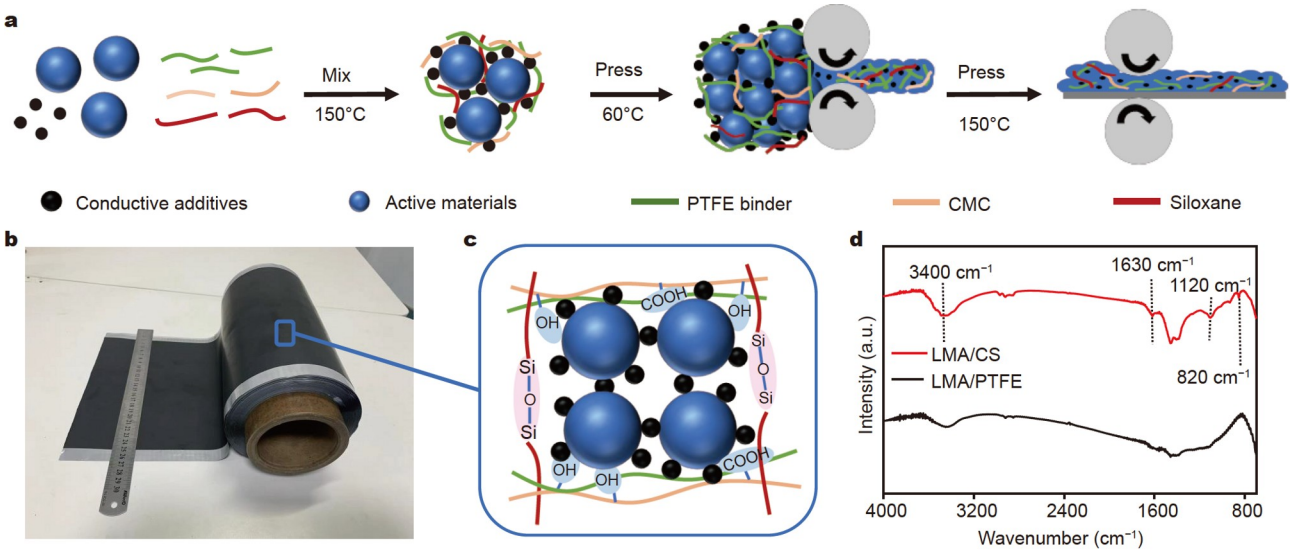

Figure 1 (a) Schematic of the fabrication procedure for the dry-processed electrode. (b) Optical photos of the prepared LMA/CS electrode film. (c) Schematic of the structural design for the LMA/CS electrode. (d) FT-IR spectra of the LMA/CS and LMA/PTFE electrodes.

mitigates crack formation, thereby conferring excellent mechanical strength to the electrode films. Consequently, this leads to improved cathode stability, thereby enhancing electrochemical performance. The Fourier-transform infrared (FT-IR) spectra of LMA/CS and LMA/PTFE electrodes are presented in Fig. 1d. The prominent bands at 1630 and 3400 cm^{-1} correspond to the stretching vibrations of C=O and C–OH, respectively. In addition, the observable bands at 1120 and 820 cm^{-1} are attributable to the asymmetric and symmetric Si–O–Si stretching vibrations, respectively [36]. The FT-IR results strongly support the successful crosslinking of CMC and siloxane within the LMA/CS electrode.

Mechanical properties and morphological characterization of the LMA/CS electrode

Fig. 2a shows the adhesion characteristics of the LMA/CS and LMA/PTFE electrodes in an electrolyte environment. The LMA/CS and LMA/PTFE electrodes were immersed in a conventional electrolyte at room temperature (25°C) for 20 min. Notably, the electrolyte remains transparent, indicating the stability of the LMA/CS and LMA/PTFE electrodes with no precipitation of cathode particles. After ultrasonic treatment for 20 s, the LMA/CS electrode remains structurally intact in the electrolyte. By contrast, the LMA/PTFE electrode exhibits significant detachment, resulting in the exposure of the current collector. The excellent mechanical stability of the LMA/CS electrode was further confirmed through a folding test. After repeated folding (1st and 2nd times), the surface of the LMA/CS electrode exhibits no significant damage (Fig. 2b). Conversely, the LMA/PTFE electrode shows significant cracks, and the LMA/PTFE electrode film detaches from the current collector. Furthermore, the stress–strain curves of the LMA/CS and LMA/PTFE electrode films were recorded (Fig. 2c). The LMA/CS electrode film shows a tensile strength of 1.32 MPa, which is considerably higher than that of LMA/PTFE (0.35 MPa). These remarkable improvements in the mechanical properties of the LMA/CS electrode can be mainly attributed to the formation of a flexible 3D Si–O–Si integrated network and the abundant functional groups of CMC. The synergistic effect of CMC and siloxane enhances the distribution of cathode materials, maintains the structural integrity of the electrode, and prevents the detachment of the electrode film from the current collector.

The scanning electron microscopy (SEM) images of the LMA/CS and LMA/PTFE electrode films are illustrated in Fig. 2d. The surface of the LMA/CS electrode exhibits a considerably smoother texture with fewer cracks and defects than the LMA/PTFE electrode. Furthermore, the LMA/CS electrode surface displays visible active material particles, whereas the LMA/PTFE electrode surface is mainly covered by binder agglomerates. This accumulation of binders on the electrode surface could hinder

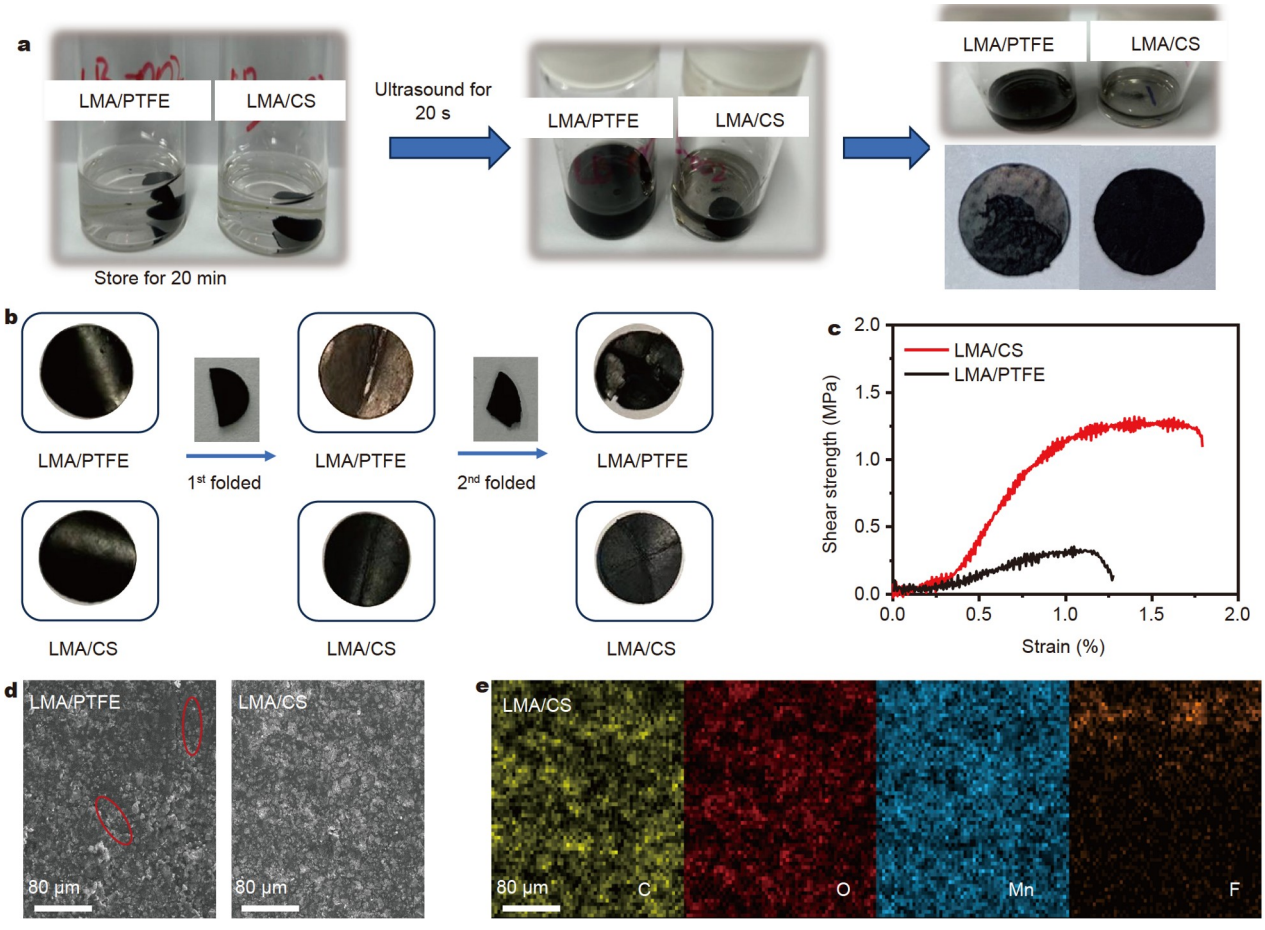

Figure 2 (a) Adhesion measurements of the LMA/PTFE and LMA/CS electrodes in the electrolyte. (b) Folding test of the LMA/PTFE and LMA/CS electrodes. (c) Comparison of the stress–strain curves of the LMA/PTFE and LMA/CS electrodes. (d) Top-view SEM images of the LMA/PTFE and LMA/CS electrodes. (e) EDS elemental mapping of the LMA/CS electrode.

the contact between the cathode components and impede Li^+ diffusion during cycling [16]. Moreover, energy-dispersive X-ray spectroscopy (EDS) tests reveal the distributions of C, O, Mn, and F (Fig. 2e and Fig. S2). The EDS spectrum of PTFE reveals the presence of F, indicating the distribution of the PTFE binder within the electrode. The EDS results reveal severe agglomeration of the PTFE binder in the LMA/PTFE electrode. This enhanced dispersion of the electrode components can be attributed to two primary factors. First, the polar functional groups originating from CMC form hydrogen bonds with the active materials, whereas the hydrophobic segments of CMC interact with the PTFE chain through hydrophobic interactions, thereby enhancing the dispersibility of the cathode components [13]. Second, the formation of a Si–O–Si network *via in-situ* crosslinking endows the electrode with high mechanical strength and inhibits crack formation.

Electrochemical performance of the LMA/CS and LMA/PTFE electrodes

To elucidate the structural advantages inherent in the LMA/CS cathode, a comparative analysis of the electrochemical performance between the LMA/CS and LMA/PTFE electrodes was conducted under identical mass loading (15.0 mg cm^{-2}). Fig. 3a, b, and Fig. S3 present the galvanostatic discharge–charge profiles of the two cathodes at 1 C, revealing similar voltage profiles of both electrodes. The LMA/CS cathode exhibits longer plateaus and lower capacity reduction than the LMA/PTFE cathode. Notably, the polarization voltage (ΔV) of the LMA/CS cathode (167–333 mV) is considerably lower than that of the LMA/PTFE cathode (200–450 mV) during each cycle. This reduced polarization voltage indicates that the interfacial contact between the components in the LMA/CS cathode is effectively enhanced [21].

The rate performance of the electrodes (Fig. 3b) demonstrates the superior rate recovery property of the LMA/CS electrode. At a rate of 0.2 C, the LMA/CS electrode achieved a specific capacity of 147.4 mA h g^{-1} (1 C = 140 mA g^{-1}), which is slightly lower than that of the LMA/PTFE electrode (166.8 mA h g^{-1}). This difference can be attributed to the relatively low conductivity of CMC and siloxane agents. As the rate switched back to 0.2 C, the LMA/CS electrode exhibited a capacity of 144.6 mA h g^{-1} with a recovery rate of 98.1%, which is higher than that of the LMA/PTFE electrode (95%). This indicates the superior reversibility of the LMA/CS electrode after testing at high rates. Subsequently, to evaluate long-term cycling performance, the LMA/CS and LMA/PTFE electrodes were operated in a voltage range of 2.0–4.3 V (*vs.* Li/Li^+) at different rates of 0.5 and 1 C, respectively (Fig. 3c, d). The LMA/CS electrode exhibits

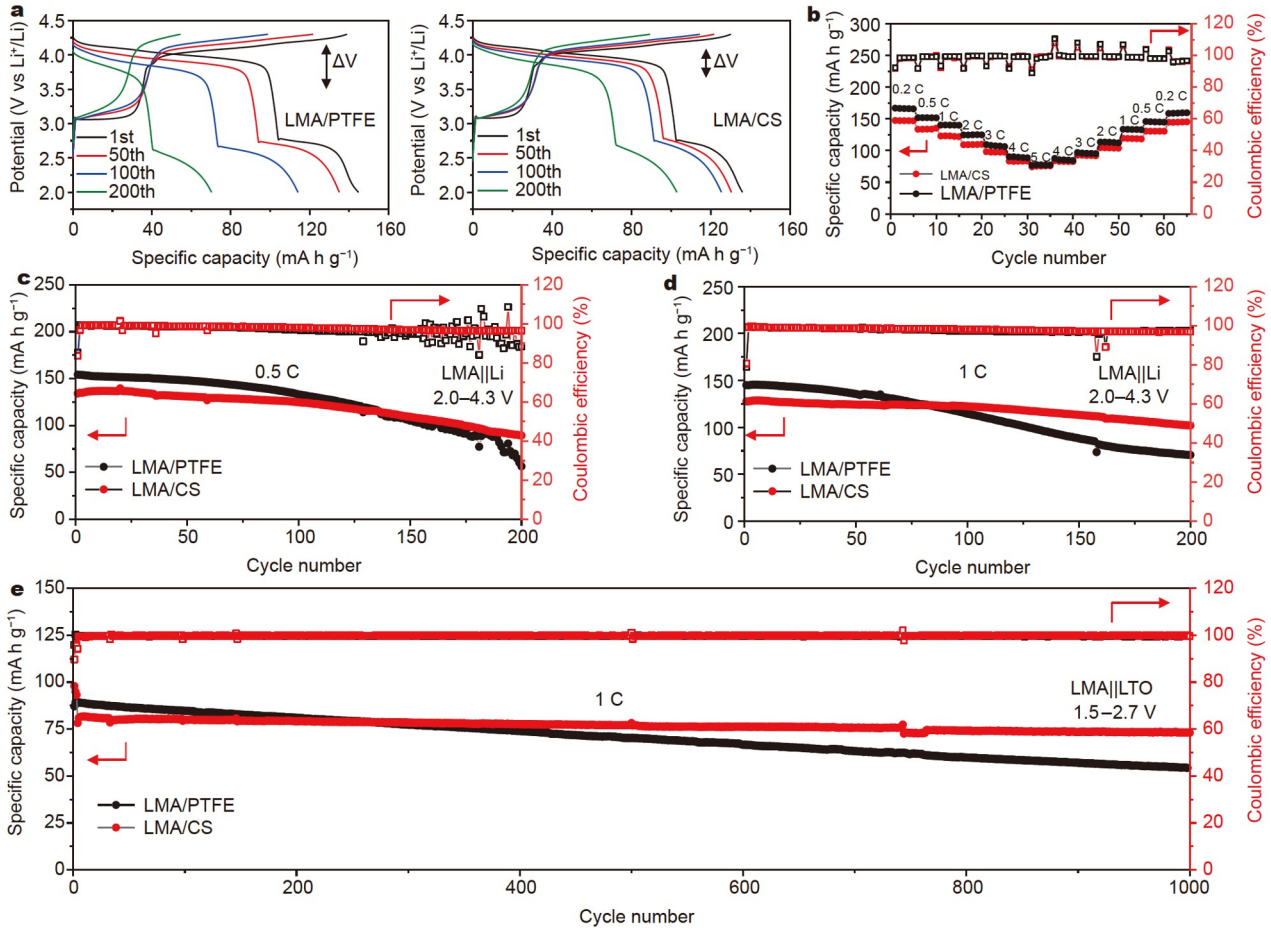

Figure 3 (a) Charge–discharge curves of the LMA/PTFE and LMA/CS dry electrodes at 1 C. (b) Rate capabilities of the LMA/PTFE and LMA/CS dry electrodes. (c) Half-cell cycling performances of the LMA/PTFE and LMA/CS dry electrodes at 0.5 C. (d) Half-cell cycling performances of the LMA/PTFE and LMA/CS dry electrodes with a mass loading of 15.0 mg cm^{-2} at 1 C. (e) Full-cell cycling performances of the LMA/PTFE||LTO and LMA/CS||LTO dry electrodes at 1 C.

an initial discharge capacity of 134 mA h g^{-1} with a capacity retention of 66.6% after 200 cycles at 0.5 C, which is considerably higher than that of the LMA/PTFE electrode (36.6%; Fig. 3c). Furthermore, the LMA/CS and LMA/PTFE electrodes exhibit initial Coulombic efficiencies (ICE) of 80.64% and 78.85%, respectively (Fig. 3d). The lower ICE of the LMA/PTFE electrode can be attributed to the PTFE binder agglomeration, which reduces the utilization rate of active materials [16]. Even after 200 cycles, the LMA/CS electrode displays an initial discharge capacity of 127.6 mA h g^{-1} and retains a capacity of 101.8 mA h g^{-1}, corresponding to a capacity retention of 79.8%. By contrast, the capacity retention of the LMA/PTFE electrode considerably decreases to 70.5 mA h g^{-1} after 200 cycles, resulting in a capacity retention of only 48.5%. Notably, the excellent cycling performance of the LMA/CS electrode substantially depends on the abundant functional groups within CMC and the formation of a 3D Si–O–Si crosslinked network. This network endows the LMA/CS electrode with excellent mechanical properties, contributing to its prolonged cycle life.

Furthermore, owing to the excellent electrochemical performance of the dry electrodes in a half-cell, a full cell (Fig. 3e) was constructed using a dry-processed LTO electrode as the anode and the LMA/CS electrode as the cathode to confirm its practical application. The LMA/CS||LTO full cell with a high mass loading (20.6 mg cm^{-2}) demonstrates excellent cycling stability at 1 C with the operating voltage range of 1.5–2.7 V. The LMA/CS||LTO full cells exhibit an initial discharge capacity of 81.8 mA h g^{-1}. After 1000 cycles, the LMA/CS||LTO cell exhibits an excellent capacity retention of 89.2%, which is considerably higher than that of the LMA/PTFE||LTO cells (only 60.9%). These results effectively verify the synergistic effect of CMC and siloxane in solvent-free dry processes for LIBs.

Teardown postmortem analysis of the LMA/CS electrode

The cross-sectional morphologies of the LMA/CS and LMA/PTFE electrodes were extensively analyzed using SEM images to elucidate the synergistic effect of CMC and the siloxane binder in suppressing the volumetric expansion of the electrodes. Fig. 4a presents the cross-sectional images of different electrodes before and after 200 cycles at 1 C. Both electrodes exhibit a similar precycling thickness. The LMA/CS electrode displays a moderate change in thickness that increases from 81 to 103 μm, indicating a small thickness increase of 27.2%. Conversely, the LMA/PTFE electrode exhibits a thickness alteration of 77.1%, which considerably exceeds that of the LMA/CS electrode. Notably, the LMA/CS cathode retains a considerably denser structure after 200 cycles, whereas the LMA/PTFE cathode exhibits multiple hollow gaps on the cross section, indicating a loose structure.

Moreover, to confirm the ability of CMC and siloxane binder to prevent the generation of electrode cracks, top-view SEM images of the LMA/CS electrode at various resolutions were examined (Fig. 4b). After 200 cycles at 1 C, the LMA/CS electrode maintains a smooth morphology with a few tiny cracks. By contrast, the LMA/PTFE electrode exhibits extensive cracks, leading to electrical contact failure among LMA particles, con-

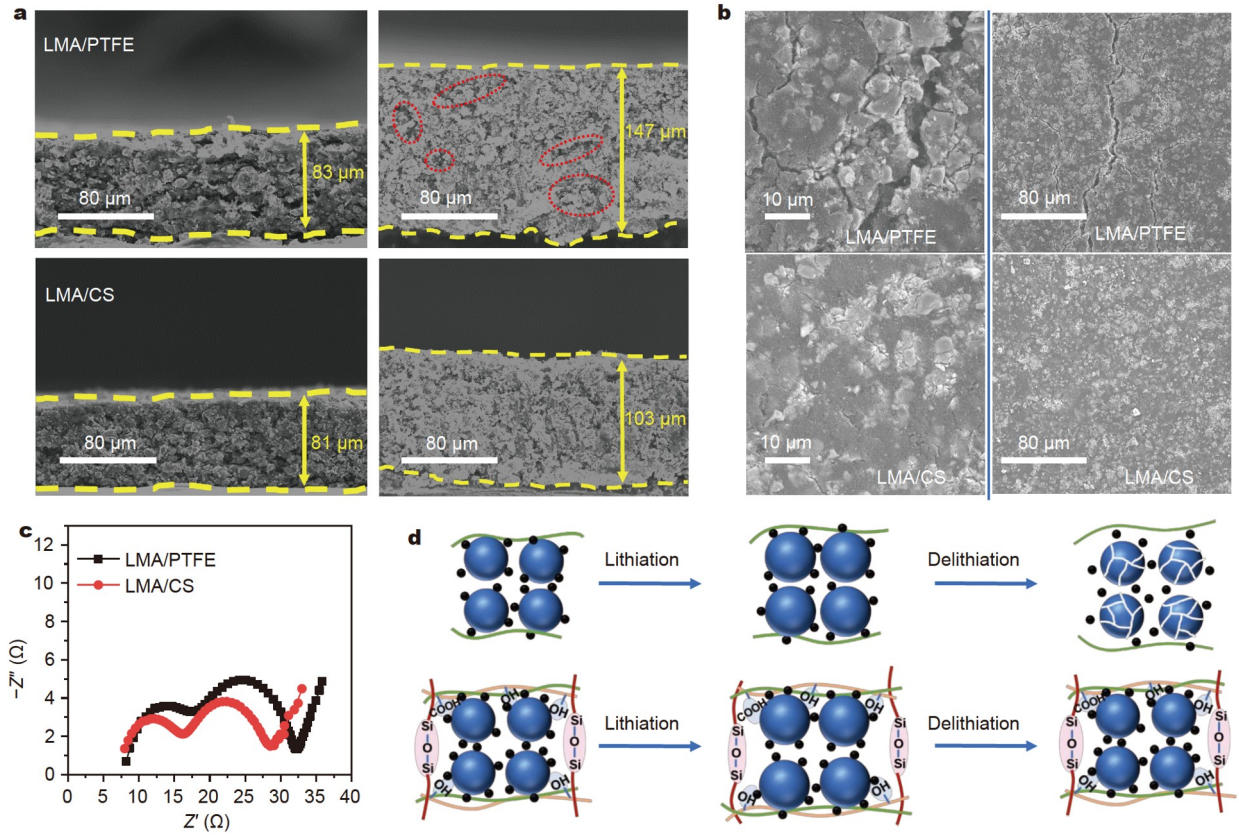

Figure 4 (a) Cross-sectional SEM images of the LMA/PTFE and LMA/CS electrodes before and after 200 cycles at 1 C. (b) Top-view SEM images of the LMA/PTFE and LMA/CS dry electrodes after 200 cycles at 1 C. (c) EIS of the LMA/PTFE and LMA/CS dry electrodes after 200 cycles at 1 C. (d) Schematic of the CMC + siloxane compared with PTFE as binders for LIBs.

ductive additives, and binders. Consequently, this results in an increase in impedance and a decrease in the electrode capacity. Generally, the strong noncovalent interactions of CMC and the formation of a 3D Si–O–Si integrated network effectively prevent the structural collapse induced by volumetric expansion. Electrochemical impedance spectroscopy (EIS) experiments were conducted before and after 200 cycles at 1 C to analyze the electron/ionic transportation behaviors of the electrodes. The LMA/CS electrode exhibits a slightly higher charge-transfer resistance (R_{CT}), as indicated by the semicircle in the medium-to-high-frequency region, than the LMA/PTFE electrode before cycling (Fig. S4). This difference is potentially attributed to the lower electrical conductivity of CMC and siloxane binder. After 200 cycles, the EIS spectra of the electrodes (Fig. 4c) exhibit two semicircles, with the semicircle in the high-frequency region representing the resistance of the CEI layer (R_{CEI}) [37]. Notably, the LMA/CS electrode exhibits smaller dimensions in both semicircles than the LMA/PTFE electrode during cycling. This suggests that CMC and siloxane binder improve the electrical contact and maintain a stable structure during cycling, consistent with the SEM results. Furthermore, after cycling, the R_{CT} of both cathodes considerably decreases, which can be attributed to the wetting of bulk active materials by the electrolyte and electrochemical activation process [38].

Fig. 4d shows the schematic of the synergistic effect of CMC and the siloxane binder in the LMA/CS cathode compared with that of the LMA/PTFE cathode. Within the LMA/CS cathode, CMC and the siloxane binder establish connections with the LMA particles through hydrogen bonds and form a 3D Si–O–Si crosslinked network. This dual bonding mechanism maintains the structural stability of the electrode and enables it to adjust to volumetric changes. During the lithiation process, LMA particles expand in volume (~10%–15% [39]); however, they effectively remain confined within the network skeleton. In the subsequent delithiation process, as the volume of LMA decreases, the LMA particles are securely held within the connected structure of CMC and siloxane through hydrogen bonds and a 3D Si–O–Si integrated network. This ensures continuous and effective contact between the LMA particles and the conductive additives, thereby preventing electric loss and capacity degradation. By contrast, owing to the limited number of polar functional groups on PTFE, PTFE could not establish a close connection with the active materials and the conductive additives. Consequently, during repeated lithiation/delithiation processes, LMA and KB particles tend to shift, resulting in uneven dispersion, poor electrical connection, and the pulverization of active materials.

To further confirm the universality of the synergistic effect of CMC and siloxane, a series of half cells were fabricated using different electrode materials, including $LiNi_{0.3}Co_{0.3}Mn_{0.3}O_2$ (NCM111, 1 C = 150 mA g^{-1}), $LiNi_{0.8}Co_{0.1}Mn_{0.1}O_2$ (NCM811, 1 C = 200 mA g^{-1}), $LiCoO_2$ (LCO, 1 C = 150 mA g^{-1}), and $Li_4Ti_5O_{12}$ (LTO, 1 C = 170 mA g^{-1}), *via* the developed dry electrode processing method. The cycling performance of these cells with CMC and the siloxane binder considerably demonstrate superior results compared with the PTFE-based electrodes. This comparative analysis is summarized in Fig. S5 and Table S1.

Morphological analysis and electrochemical performance comparisons of the dry-processed LMA/CS and slurry-based LMA/PVDF electrodes

The LMA/PVDF electrode was fabricated *via* conventional slurry-processed methods, which involved the blending of LMA particles, conductive additives, and binders in NMP. Subsequently, the slurry was coated onto the carbon-coated Al foil, dried, and finally calendared [40]. The LMA/PVDF electrode comprises LMA, KB, and the PVDF binder in a mass ratio of 85:10:5. Compared with the LMA/PVDF electrode, the dry-processed LMA/CS electrode exhibits structural superiority and higher cycling stability (Fig. 5).

Moreover, we focused on the comparison between the LMA/CS electrode with a mass loading of 15.0 mg cm^{-2} and the LMA/PVDF electrode with a mass loading of 8.7 mg cm^{-2}. The electrochemical performances of the LMA/PVDF and LMA/CS electrodes were evaluated at 1 C in half cells. The galvanostatic cycling performances (Fig. 5a) reveal that the LMA/PVDF electrode shows an initial discharge capacity of 120.8 mA h g^{-1}, slightly lower than that of the LMA/CS electrode. However, the capacity of the LMA/PVDF electrode sharply decreases over 200 cycles, with a capacity retention of only 59.7%. By contrast, the LMA/CS electrode exhibits a superior capacity retention of 79.8%. The lower initial capacity and rapid capacity loss observed in the LMA/PVDF cathode can be attributed to the insufficient adhesion strength of PVDF, which lacks sufficient functional groups to maintain a connection with the conductive additives after the volumetric expansion of LMA particles.

Fig. 5b displays the long-cycle discharge curves of full cells based on a dry-processed LTO electrode as the anode at 1 C. During repeated lithiation/delithiation processes, the brittle PVDF binder is unable to accommodate the stress induced by volume variation, resulting in a significant decrease in overall performance. After ~550 cycles, the capacity of the LMA/PVDF electrode nearly decays to 0. By contrast, the LMA/CS electrode exhibits superior long-cycling performance with an excellent capacity retention of 89.2% after 1000 cycles.

Fig. S6 illustrates the rate performance of the LMA/PVDF electrode. At the rate of 5 C, the LMA/PVDF exhibits a capacity of 70.1 mA h g^{-1}, whereas the LMA/CS electrode demonstrates a higher capacity of 75.8 mA h g^{-1} (Fig. 3b). The presence of cracks resulting from solvent evaporation in the LMA/PVDF electrode could hinder Li^+ diffusion along the thickness direction, thereby diminishing the rate performance, particularly at higher rates. By contrast, the LMA/CS electrode with a denser structure, provides a shorter Li^+ diffusion pathway, thereby promoting fast-charging performance [41]. To provide strong evidence for this conclusion, the cross-sectional morphologies of the LMA/PVDF electrode were further examined using SEM images (Fig. S7). Despite the similar thickness change (26.7%, from 60 to 76 μm) of the LMA/PVDF electrode compared with the LMA/CS electrode (27.2%), the LMA/PVDF electrode exhibits numerous visible cracks and hollows. These structural imperfections in the LMA/PVDF electrode lead to a weakened electronic percolation network and a reduction in high-rate performance.

Furthermore, the morphologies of the LMA/CS and LMA/PVDF electrodes with varying mass loadings were examined using the top-view SEM images (Fig. 5c). As the mass loading increased, the surface of the LMA/PVDF electrode exhibited considerable cracks and hollows, whereas the LMA/CS electrode maintained a smooth and crack-free surface. This result can be attributed to capillary action and diffusion effects during solvent evaporation, which lead to the aggregation of the binder and the conductive additives [42].

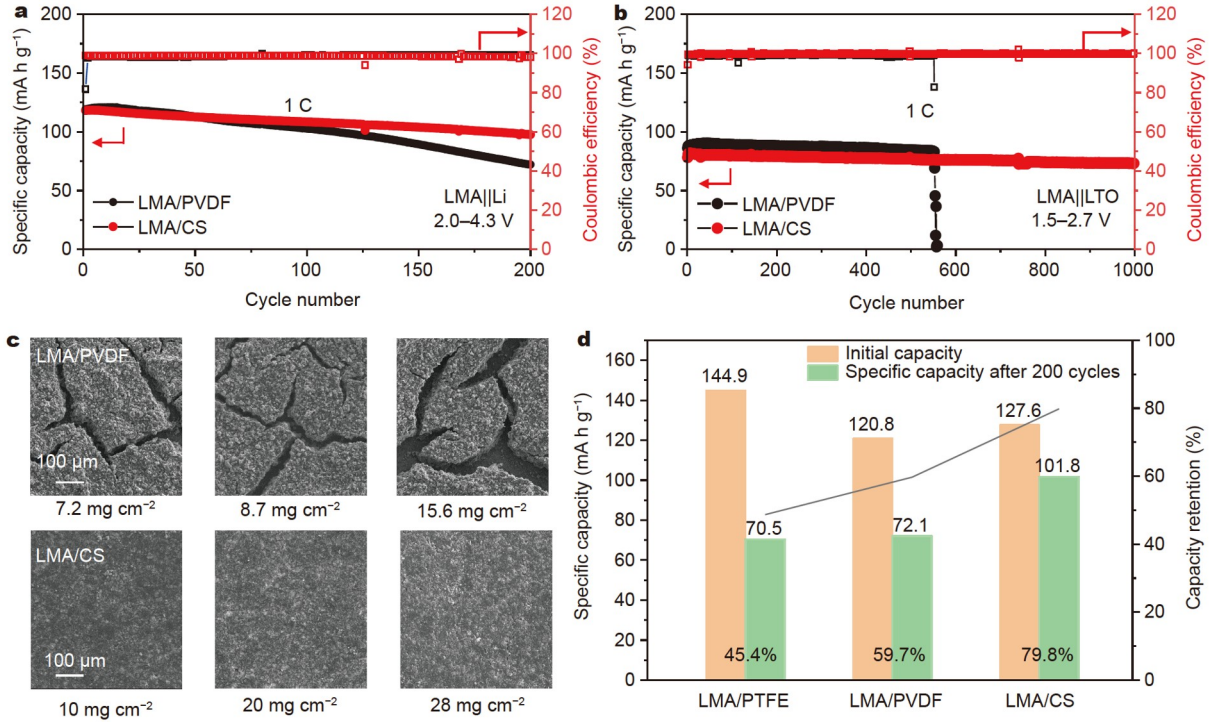

Figure 5 (a) Half-cell cycling performances of the LMA/PVDF and LMA/CS electrodes at 1 C. (b) Full-cell cycling performances of the LMA/PVDF and LMA/CS electrodes at 1 C. (c) Top-view SEM images of the LMA/PVDF and LMA/CS electrodes before cycling with different mass loadings. (d) Comparison of half-cell performance with different electrodes (LMA/PTFE, LMA/PVDF, and LMA/CS) before and after 200 cycles at 1 C.

Fig. 5d shows an overview of the half-cell cycling performance of the three electrodes with different binders. The remarkable cycling stability of the LMA/CS electrode is mainly attributed to the synergistic effect of CMC and siloxane crosslinker. First, the substantial polar functional groups of CMC form hydrogen bonding interactions with the active materials, whereas the hydrophobic segments of CMC interacte with the PTFE chain through hydrophobic interactions. This results in an improved distribution of cathode components and enhances the mechanical strength of the electrode film [43]. Second, the formation of the Si–O–Si integrated network by *in-situ* crosslinking endows the electrodes with high flexibility. This property allows the electrodes to effectively accommodate severe volumetric expansion and maintain structural integrity throughout repeated charge–discharge cycles.

CONCLUSIONS

An industrially viable solvent-free dry process for producing LIB electrodes was successfully developed using the synergistic effect of CMC and siloxane agents. The polar functional groups of CMC enhanced the distribution of the cathode components and improved the mechanical integrity of the electrodes. Moreover, siloxane readily formed a Si–O–Si network, which effectively mitigated volumetric changes and reduced crack formation, thereby enhancing the structural stability of the electrode. Consequently, the prepared LMA/CS dry electrode exhibited an excellent capacity retention of 79.8% after 200 cycles at 1 C. In addition, the LMA/CS||LTO full cell, with a high mass loading of 20.6 mg cm^{-2}, demonstrated excellent electrochemical stability with a capacity retention of 89.2% after 1000 cycles. This indicates a substantial enhancement in the cycling stability of the LMA/CS cell compared with that based on the LMA/PTFE and LMA/PVDF electrodes. Furthermore, the excellent compatibility of the LMA/CS||LTO cell with other commercial active materials makes it a cost-effective and eco-friendly solution for the large-scale industrial production of LIB electrodes.

Received 18 September 2023; accepted 30 October 2023; published online 11 December 2023

1 Quilty CD, Wu D, Li W, *et al.* Electron and ion transport in lithium and lithium-ion battery negative and positive composite electrodes. Chem Rev, 2023, 123: 1327–1363
2 Lu Y, Rong X, Hu YS, *et al.* Research and development of advanced battery materials in China. Energy Storage Mater, 2019, 23: 144–153
3 Zhou G, Li F, Cheng HM. Progress in flexible lithium batteries and future prospects. Energy Environ Sci, 2014, 7: 1307–1338
4 Zhong W, Zhang C, Li S, *et al.* Mo_2C catalyzed low-voltage prelithiation using nano-$Li_2C_2O_4$ for high-energy lithium-ion batteries. Sci China Mater, 2022, 66: 903–912
5 Xu L, Sun Z, Zhu Y, *et al.* A Li-rich layered-spinel cathode material for high capacity and high rate lithium-ion batteries fabricated *via* a gas-solid reaction. Sci China Mater, 2020, 63: 2435–2442
6 Ryu M, Hong YK, Lee SY, *et al.* Ultrahigh loading dry-process for solvent-free lithium-ion battery electrode fabrication. Nat Commun, 2023, 14: 1316
7 Zhang Z, Sun S, Zhang W, *et al.* Internally inflated core-buffer-shell structural Si/EG/C composites as high-performance anodes for lithium-ion batteries. Sci China Mater, 2022, 65: 2949–2957
8 Pettinger KH, Dong W. When does the operation of a battery become environmentally positive? J Electrochem Soc, 2017, 164: A6274–A6277
9 Liu Y, Zhang R, Wang J, *et al.* Current and future lithium-ion battery manufacturing. iScience, 2021, 24: 102332
10 Degen F, Winter M, Bendig D, *et al.* Energy consumption of current and future production of lithium-ion and post lithium-ion battery cells. Nat Energy, 2023, 8: 1284–1295
11 Agarwal RG, Coste SC, Groff BD, *et al.* Free energies of proton-coupled electron transfer reagents and their applications. Chem Rev, 2021, 122:

1–49
12 Yao W, Chouchane M, Li W, *et al.* A 5 V-class cobalt-free battery cathode with high loading enabled by dry coating. Energy Environ Sci, 2023, 16: 1620–1630
13 Lingappan N, Kong L, Pecht M. The significance of aqueous binders in lithium-ion batteries. Renew Sustain Energy Rev, 2021, 147: 111227
14 Zhang Z, Zeng T, Qu C, *et al.* Cycle performance improvement of $LiFePO_4$ cathode with polyacrylic acid as binder. Electrochim Acta, 2012, 80: 440–444
15 Li Y, Wu Y, Wang Z, *et al.* Progress in solvent-free dry-film technology for batteries and supercapacitors. Mater Today, 2022, 55: 92–109
16 Liu Y, Gong X, Podder C, *et al.* Roll-to-roll solvent-free manufactured electrodes for fast-charging batteries. Joule, 2023, 7: 952–970
17 Kato Y, Shiotani S, Morita K, *et al.* All-solid-state batteries with thick electrode configurations. J Phys Chem Lett, 2018, 9: 607–613
18 Abdollahifar M, Cavers H, Scheffler S, *et al.* Insights into influencing electrode calendering on the battery performance. Adv Energy Mater, 2023, 13: 2300973
19 Tao R, Steinhoff B, Sun XG, *et al.* High-throughput and high-performance lithium-ion batteries *via* dry processing. Chem Eng J, 2023, 471: 144300
20 Wang C, Yu R, Duan H, *et al.* Solvent-free approach for interweaving freestanding and ultrathin inorganic solid electrolyte membranes. ACS Energy Lett, 2021, 7: 410–416
21 Hong SB, Lee YJ, Kim UH, *et al.* All-solid-state lithium batteries: Li^+-conducting ionomer binder for dry-processed composite cathodes. ACS Energy Lett, 2022, 7: 1092–1100
22 Tao R, Tan S, Meyer III HM, *et al.* Insights into the chemistry of the cathodic electrolyte interphase for PTFE-based dry-processed cathodes. ACS Appl Mater Interfaces, 2023, 15: 40488–40495
23 Nirmale TC, Kale BB, Varma AJ. A review on cellulose and lignin based binders and electrodes: Small steps towards a sustainable lithium ion battery. Int J Biol Macromolecules, 2017, 103: 1032–1043
24 Teng X, Fang W, Liang Y, *et al.* High-performance polyamide nanofiltration membrane with arch-bridge structure on a highly hydrated cellulose nanofiber support. Sci China Mater, 2020, 63: 2570–2581
25 Liang Y, Wei Z, Wang H-E, *et al.* Flexible freestanding conductive nanopaper based on PPy:PSS nanocellulose composite for supercapacitors with high performance. Sci China Mater, 2022, 66: 964–973
26 Lux SF, Schappacher F, Balducci A, *et al.* Low cost, environmentally benign binders for lithium-ion batteries. J Electrochem Soc, 2010, 157: A320
27 Buqa H, Holzapfel M, Krumeich F, *et al.* Study of styrene butadiene rubber and sodium methyl cellulose as binder for negative electrodes in lithium-ion batteries. J Power Sources, 2006, 161: 617–622
28 Ma C, Wen Y, Qiao Q, *et al.* Improving electrochemical performance of high-voltage spinel $LiNi_{0.5}Mn_{1.5}O_4$ cathodes by silicon oxide surface modification. ACS Appl Energy Mater, 2021, 4: 12201–12210
29 Meng J, Chu F, Hu J, *et al.* Liquid polydimethylsiloxane grafting to enable dendrite-free Li plating for highly reversible Li-metal batteries. Adv Funct Mater, 2019, 29: 1902220
30 Oh I, Cho J, Kim K, *et al.* Poly(imide-*co*-siloxane) as a thermo-stable binder for a thin layer cathode of thermal batteries. Energies, 2018, 11: 3154
31 Wang H, Zhang X, Li Y, *et al.* Siloxane-based organosilicon materials in electrochemical energy storage devices. Angew Chem Int Ed, 2022, 61: e202210851
32 Kim HJ, Kim JS, Song SW. Uniform distribution of siloxane-grafted SiO nanoparticles in micron hard-carbon matrix for high-rate composite anode in Li-ion batteries. J Solid State Chem, 2019, 270: 479–486
33 Teng P, Wang Z, Kang Y, *et al.* Metal-ion-tunable adhesive elastomers for mounting the multilayer elastic circuit. Sci China Mater, 2023, 66: 4054–4061
34 Hippauf F, Schumm B, Doerfler S, *et al.* Overcoming binder limitations of sheet-type solid-state cathodes using a solvent-free dry-film approach. Energy Storage Mater, 2019, 21: 390–398
35 Kim SW, Kim T, Kim YS, *et al.* Surface modifications for the effective dispersion of carbon nanotubes in solvents and polymers. Carbon, 2012, 50: 3–33
36 Wang Y, Dong N, Liu B, *et al.* Self-adaptive gel poly(imide-siloxane) binder ensuring stable cathode-electrolyte interface for achieving high-performance NCM811 cathode in lithium-ion batteries. Energy Storage Mater, 2023, 56: 621–630
37 Li Z, Wu G, Yang Y, *et al.* An ion-conductive grafted polymeric binder with practical loading for silicon anode with high interfacial stability in lithium-ion batteries. Adv Energy Mater, 2022, 12: 2201197
38 Yao Q, Zhu Y, Zheng C, *et al.* Intermolecular cross-linking reinforces polymer binders for durable alloy-type anode materials of sodium-ion batteries. Adv Energy Mater, 2022, 13: 2202939
39 Deng S, Wang H, Liu H, *et al.* Research progress in improving the rate performance of $LiFePO_4$ cathode materials. Nano-Micro Lett, 2014, 6: 209–226
40 Al-Shroofy M, Zhang Q, Xu J, *et al.* Solvent-free dry powder coating process for low-cost manufacturing of $LiNi_{1/3}Mn_{1/3}Co_{1/3}O_2$ cathodes in lithium-ion batteries. J Power Sources, 2017, 352: 187–193
41 Daemi SR, Tan C, Volkenandt T, *et al.* Visualizing the carbon binder phase of battery electrodes in three dimensions. ACS Appl Energy Mater, 2018, 1: 3702–3710
42 Font F, Protas B, Richardson G, *et al.* Binder migration during drying of lithium-ion battery electrodes: Modelling and comparison to experiment. J Power Sources, 2018, 393: 177–185
43 Ahn J, Im HG, Lee Y, *et al.* A novel organosilicon-type binder for $LiCoO_2$ cathode in Li-ion batteries. Energy Storage Mater, 2022, 49: 58–66

Acknowledgements This work was supported by the National Natural Science Foundation of China (52090034), the Ministry of Science and Technology of China (2020YFA0711500), and the Higher Education Discipline Innovation Project (111 Project B12015).

Author contributions Zhang H conceived and designed the research; Ni M fabricated the electrodes and assembled the cells; Ni M, Zhao Y and Xu N conducted the characterizations and analyses with support from Kong M, Ma Y and Li C; Ni M and Zhang H wrote the paper with support from Chen Y; Chen Y and Zhang H coordinated the study. All authors contributed to the general discussion.

Conflict of interest The authors declare that they have no conflict of interest.

Supplementary information Experimental details and supporting data are available in the online version of the paper.

Minghan Ni received her BS degree in materials science and engineering from China University of Geoscience (Beijing). Currently, she is pursuing her Master's degree at Nankai University under the guidance of Prof. Yongsheng Chen. Her research is primarily focused on improving the electrochemical performances and mechanical properties of dry-processed LIBs.

Hongtao Zhang received his PhD degree from the Institute of Chemistry, Chinese Academy of Sciences in 2012. He joined Prof. Yongsheng Chen's group at Nankai University in 2014. He worked as a visiting scholar at the University of California, Los Angeles from 2018 to 2019. His current research primarily centers on polymer solid electrolytes and high-performance lithium metal batteries.

Yongsheng Chen graduated from the University of Victoria with a PhD degree in chemistry in 1997 and then joined the University of Kentucky and the University of California, Los Angeles for postdoctoral reseach from 1997 to 1999. Since 2003, he has been a chair professor at Nankai University. His main research interests include (i) carbon-based nanomaterials, including carbon nanotubes and grapheme, (ii) organic and polymeric functional materials, and (iii) energy devices including organic photovoltaics and supercapacitors.

通过羧甲基纤维素和硅氧烷的协同作用提升锂离子电池干法正极的循环稳定性

倪铭韩[1,3], 赵阳[1,3], 许诺[1,3], 孔萌昕[4], 马延风[1,3], 李晨曦[1,3], 张洪涛[1,3*], 陈永胜[1,2,3]

摘要 近年来，无溶剂干法电极制备工艺由于其低成本和低污染等优点在锂电池领域获得了广泛关注. 然而, 现有干法制备工艺中采用的聚四氟乙烯(PTFE)粘结剂存在粘附力和循环稳定性不足等缺点，限制了其实际工业化应用. 我们通过引入羧甲基纤维素(CMC)和硅氧烷作为粘结剂复合材料，发展了一种与现有工业化生产兼容的锂离子电池干法电极制备工艺. CMC和硅氧烷的协同作用增强了电极活性材料的粘附性能, 实现了干法电极膜片机械强度和电化学性能的大幅提升. 基于这种干法电极工艺制备的铝掺杂锰酸锂(LMA/CS)半电池在1 C下循环200圈后展示出79.8%的保持率. 进一步地, 制备的高负载(20.6 mg cm^{-2})锰酸锂-钛酸锂全电池(LMA/CS||LTO)实现了1000圈的超长稳定循环, 容量保持率高达89.2%，超过现有基于PTFE粘结剂干法工艺和传统湿法工艺的电池性能.